MATERIALE PLASTICE
https://revmaterialeplastice.ro
https://doi.org/10.37358/Mat.Plast.1964

Experimental Analysis of Hyperelastic Materials Using the Vibration Method

MIRUNA CIOLCA https://orcid.org/0009-0006-9984-946X**,**
DANIEL VLASCEANU* https://orcid.org/0000-0002-6609-7496
National University of Science and Technology Politehnica Bucharest, Department of Strength of Materials, 313 Splaiul Independentei, 060042, Bucharest, Romania

Abstract: *The elaborated paper presents a series of methodologies with which the dynamic characteristics (damping coefficient, damping factor) can be determined, depending on the working conditions, of a hyperelastic material using vibration theory. These methodologies can be extended to characterize any type of hyperelastic material. The main aim of this work is to develop experimental technology and methodology to characterize this type of materials like rubber to establish a series of dynamic factors like damping factor, transmissibility at resonance, pulsation at resonance, dynamic elastic constant. These characteristics are variable, depending on composition, request, etc. In conclusion, they are not available in specialized literature as are the characteristics of linear-elastic materials. The application of numerical calculation programs in carrying out resistance calculations, in the case of structures made of such materials, is also impossible to achieve, having as an impediment the lack of knowledge of the values of the material characteristics.*

Keywords: *rubber, damping coefficient, transmissibility, dynamic characteristics, vibration, frequency*

1. Introduction

The study regarding hyperelastic materials and their characteristics determination are of great importance as shown also in specialty literature, demonstrated by the increase of published works starting from 1990 to present [1]. Hyperelastic materials, referred also as green elastic materials, are defined by their deformation energy relations [2].

The foundation of this research was made by studying the work of Boyce and Arruda, in which statistical and continuum mechanics models of incompressible rubber elasticity are compared to experimental data [3]. Boyce and Arruda compared five models, based on the experimental work of Treloar, for three types of deformation: uniaxial, biaxial, pure shear [4].

Marckmann and Verron had an extensive study comparing twenty hyperelastic models for rubber-like materials, in which all elastomers that were used are assumed iso-tropic and incompressible and viscoelasticity, stress-softening, damage were not taken into account [5]. This study aimed to classify the elastomers as per their ability to fit ex-perimental data and to improve the formulas used for finite element simulations.

In order to dynamically model the assemblies containing elements made of hypere-lastic materials (car pivot, couplings, insulation elements and others), material characteristics are required that must be determined experimentally [6]. There are four hyperelastic models that are frequently used when characterizing these materials: Neo Hookean, Mooney-Rivlin, Ogden and Yeoh [7-9].

The dynamic characteristics of hyperelastic materials are a priority when designing parts containing these kinds of materials, mostly from the transmissibility point of view [10]. Melly. et al presented a review of fifteen hyperelastic models that were very useful in understanding the complex mechanical properties of the studied materials and in de-signing complex engineering assemblies [11]. Somarathna. et al deepened a study about a viscoelastic model, under varying strain rate conditions, which combines one set of hy-perelastic model parameters with viscoelastic model parameters [12]. The proposed model resulted in accuracy for predicting the material behavior.

**email: daniel.vlasceanu@upb.ro*

Wang et al used the Dynamic Mechanical Analysis characteristics and experiments to study the influence of damping materials on structural vibration, in diverse working conditions [13]. The research aims to define a base for manufacturing intelligent damping materials.

Using vibration theory, the paper establishes and uses a methodology, developed by the authors, for determining dynamic characteristics, applied to the study of two types of hyperelastic materials different by the percentage of natural rubber quantity. Both materials are obtained by vulcanization process.

In order to determine the dynamic characteristics and verify their variation depending on the composition of the hyperelastic material, the behavior of two types of materials with different compositions, coded C40 and respectively C80, was studied.

2. Materials and methods

2.1. Determination of the complex elastic constant of rubber

The study was conducted analyzing two hyperelastic materials (rubber) with different chemical composition, namely:

• Material I – code C40 – mixture of 40% natural rubber and 60% recycled rubber (re-generated rubber).

• Material II – code C80 – mixture of 80% natural rubber and 20% active white filler (silica).

Analyzing a system like the one in Figure 1, it must be equated with derived systems, which, using classical dynamic analysis methods, can be characterized according to the intended use of the product.

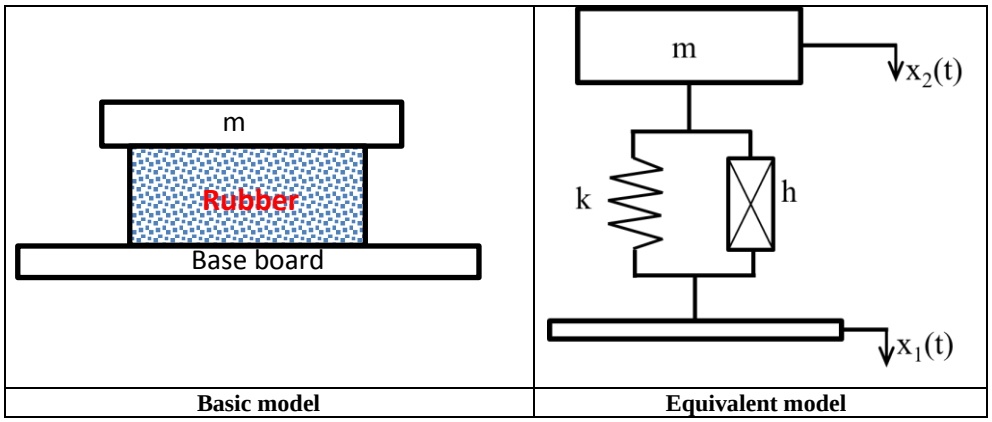

Figure 1. Experimental model

In Figure 1, the rubber is modeled by the spring with dynamic elastic constant, *k*, and by the damper, with hysteretic damping coefficient, *h*, connected in parallel with the spring.

The rubber is fixed by bonding between an upper rigid mass and the base board, which has a harmonic translational motion $x_1(t)$. Analyzing the dynamic response of the upper mass $x_2(t)$, there can be established the relations for the calculation of the rubber dynamic characteristics, which presents both elastic and dissipative characteristics [14].

If the damping force is proportional to the relative displacement of the ends of the damper (rubber) and in phase with the velocity, and the energy dissipated per vibration cycle does not depend on the frequency, the complex elastic constant of the rubber has the expression [15]:

$$k^* = k + ih = k(1 + ig) \tag{1}$$

where $g = h/k$ is the hysteretic damping factor of the rubber.

The motion equation of mass *m* is:

$$m\ddot{x} + k^*(x_2 - x_1) = 0 \tag{2}$$

If the harmonic displacement is:

$$x_1(t) = X_1 e^{i\omega t} \tag{3}$$

then mass *m* will have, in stationary mode, a harmonic displacement as:

$$x_2(t) = X_2^* e^{i\omega t} = X_2 e^{i(\omega t - \varphi)} \quad (4)$$

where x_1 and x_2 are the amplitudes of the two displacements, and φ represents the phase difference between them.

By substituting relations (4) and (3) into equation (2), it is obtained the complex transmissibility of motion:

$$T^* = \frac{X_2^*}{X_1} = \frac{k^*}{k^* - m\omega^2} = \frac{1+ig}{1-\left(\frac{\omega}{p}\right)^2 + ig} \quad (5)$$

where:

$$p = \sqrt{\frac{k}{m}} \quad (6)$$

The terms in relation (1), which express the complex elastic constant of rubber, can be determined by various methods.

2.1.1. Transmissivity method (maximum amplitude method)

The method involves measuring the amplitudes x_1 and x_2 (Figure 1 and relations (3) and (4)) and calculating the transmissibility modulus as a ratio of the two amplitudes, at different values of the excitation pulse, ω [16].

$$T = |T^*| = \frac{X_2}{X_1} = \sqrt{\frac{1+g^2}{\left(1-\frac{\omega^2}{p^2}\right)^2 + g^2}} \quad (7)$$

The maximum value of transmissibility T_{max} corresponds to resonance, when $\omega = p$.

Knowing this pulsation, *p*, is calculated the dynamic elastic constant:

$$k = mp^2 \quad (8)$$

The ordinate points $\frac{1}{\sqrt{2}}T_{max}$, also called half-power points, have abscissas:

$$\omega_{1,2} = p\sqrt{1 \pm g} \quad (9)$$

The damping factor, *g*, is calculated with the following relations:

$$g = \frac{\omega_2^2 - \omega_1^2}{\omega_2^2 + \omega_1^2} = \frac{\omega_2^2 - \omega_1^2}{2p^2} \quad (10)$$

At resonance, when $\omega = p$,

$$T_{max} = \frac{1}{g}\sqrt{1+g^2} \quad (11)$$

for the calculation of *g*, it can also be used the following relation:

$$g = \frac{1}{\sqrt{T_{max}^2 - 1}} \quad (12)$$

The values of the damping factor, *g*, and the dynamic elastic constant, *k*, thus determined are used in relation (1) to determine the complex elastic constant of the rubber, k^* [17].

2.1.2. Phase shift diagram method

The measuring stand used in the phase shift diagram method is shown in Figure 2.

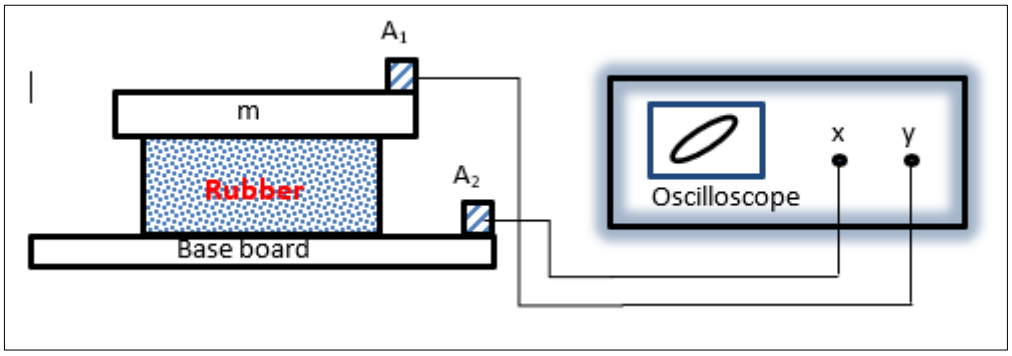

Figure 2. Measuring stand

It is considered that *x* and *y* are the signals obtained from the two accelerometers A_1 and A_2. They are of the form:

$$x = A \sin \omega t$$
$$y = A \sin(\omega t + \varphi) \quad (13)$$

if at each working frequency ω, the amplification on the two measurement channels is adjusted, so that the displacements of the spots on the oscilloscope screen are equal in the two directions.

By eliminating time from expressions (13), it is obtained the equation of the ellipse that appears on the oscilloscope screen:

$$x^2 + y^2 - 2xy \cos \varphi = A^2 \sin^2 \varphi \quad (14)$$

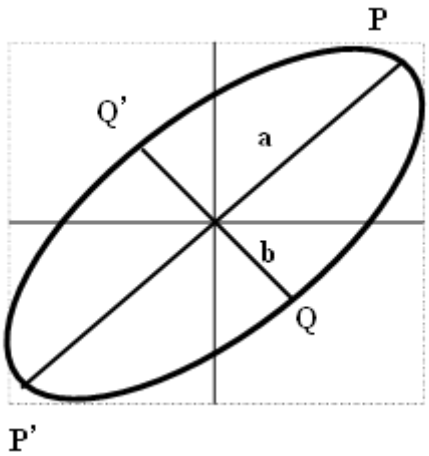

Figure 3. Scheme of oscilloscope spots

It is considered that *a* and *b* are the semi-axes of this ellipse (Figure 3). In point *P*, $x = y = \frac{a}{\sqrt{2}}$. Inserting these values into equation (14), it results:

$$a^2 = \frac{A^2 sin^2 \varphi}{1 - cos\varphi} \quad (15)$$

In point *Q*, $x = y = \frac{b}{\sqrt{2}}$, substituting in equation (14), it results:

$$b^2 = \frac{A^2 sin^2 \varphi}{1 + cos\varphi} \quad (16)$$

Using relations (15) and (16), it is obtained:

$$\frac{b}{a} = \sqrt{\frac{1-cos\varphi}{1+cos\varphi}} = tg\frac{\varphi}{2} \tag{17}$$

From relation (17), it can be concluded that the phase shift:

$$\varphi = 2arctg\frac{b}{a} \tag{18}$$

can be calculated by measuring the ellipse axes a and b in Figure 3.

By repeating the measurements for several frequencies, in the vicinity of the resonance, it is represented a diagram as shown in Figure 4.

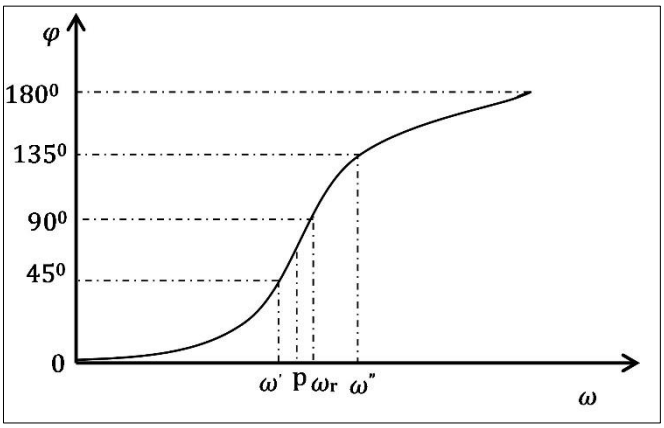

Figure 4. Diagram of phase shift as a function of frequency

From the complex transmissibility of the motion *T** (relation (5)), the phase shift is obtained:

$$\varphi = arctg\frac{g\left(\frac{\omega}{p}\right)^2}{1-\frac{\omega^2}{p^2}+g^2} \tag{19}$$

The ordinate points of 45^o and 135^o have the pulsations as abscissas:

$$\omega', \omega'' = p\sqrt{\frac{1+g^2}{1\pm g}} \tag{20}$$

This results in the damping factor:

$$g = \frac{(\omega'')^2-(\omega')^2}{(\omega'')^2+(\omega')^2} \tag{21}$$

The ordinate point of 90^o has the abscissa:

$$\omega_r = p\sqrt{1+g^2} \tag{22}$$

This results in the dynamic elastic constant:

$$k = mp^2 = \frac{m\omega_r^2}{1+g^2} \tag{23}$$

Following the calculation performed with relations (21) and (23), the complex elastic constant is obtained with relation (1).

2.1.3. Polar diagram method

The complex transmissibility can be written as:

$$T^* = T_R + iT_i \tag{24}$$

The real and imaginary parts result:

$$T_R = \frac{1-\frac{\omega^2}{p^2}+g^2}{\left(1-\frac{\omega^2}{p^2}\right)^2+g^2} \tag{25}$$

and

$$T_i = \frac{-g\frac{\omega^2}{p^2}}{\left(1-\frac{\omega^2}{p^2}\right)^2+g^2} \tag{26}$$

Eliminating the pulsation ω between the real part T_R and the imaginary part T_i results a polar curve (Niquist-type):

$$\left(T_R-\frac{1}{2}\right)^2+\left(T_i-\frac{1}{2g}\right)^2=\frac{1+g^2}{4g^2} \tag{27}$$

This polar diagram represents the geometric locus of the extremity of the vector T^* in the complex plane (Figure 5) [16].

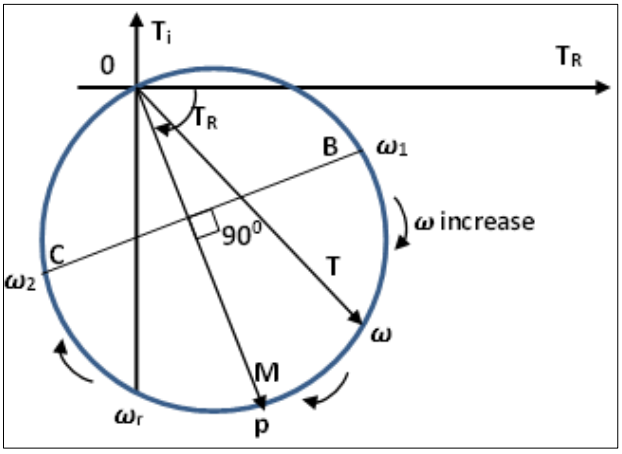

Figure 5. Polar diagram of Niquist-type

Because the transmissibility is maximum at resonance, the point *M*, of maximum amplitude, defines the pulsation *p*. The diameter *BC*, perpendicular to *OM*, defines the half-power points, of pulsations ω_1 and ω_2.

With the values of the ratio of the amplitudes of the accelerations equal to those of the ratio of the amplitudes of the displacements (harmonic motion):

$$\frac{\ddot{X}_2}{\ddot{X}_1}=\frac{\omega^2 X_2}{\omega^2 X_1}=\frac{X_2}{X_1}=T \tag{28}$$

and of the phase shift φ, determined for different disturbing frequencies, the coordinate points $T_R=T\cos\varphi$ and $T_i=T\sin\varphi$ are plotted. A "best fit" circle is drawn through these points, resulting a polar diagram like the one in Figure 5.

At point M, of maximum amplitude, the resonance frequency is determined. The diameter BC is drawn perpendicular to OM and thus are determined the frequencies of the half-power points. Then *k* and *g* are calculated, with relations (8) and (9), and the complex elastic constant, with relation (1).

2.2. Testing equipment

The experimental tests were carried out in a Vibration Laboratory using the following equipment, as shown in Figure 6.

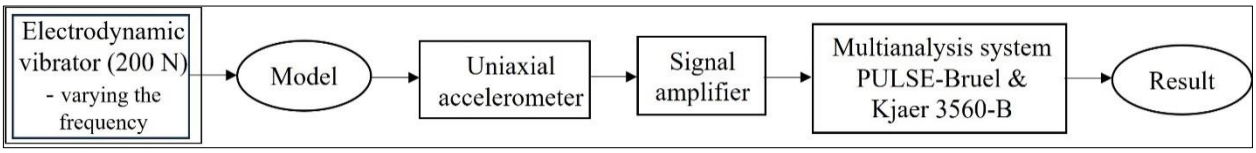

Figure 6. Testing equipment for vibration test

3. Results and discussions

3.1. Determination of transmissibility, *T*, for the studied hyperelastic materials

For to determine the frequency-transmissibility dependence, the system shown in Figure 7 was created, as follows:

- the upper component of mass m=0.5 kg, to which is added the mass of the piezoelectric accelerometer, approximately 0.1 kg;
- the elastic component – rubber (C40) – cylindrical shape, diameter ⌀=78mm and height h= 20 mm;
- the base board.

Figure 7. Transmissibility measurement chain as a function of frequency

The conduct of the experiment consisted in determining, in advance, the resonance frequency. To determine the frequency-transmissibility dependence, the frequency was varied, around the resonance value, and with the help of the multi-analysis system, the signal amplitudes in the *OX* and *OY* directions were recorded [18-20].

During the experiment there were obtained the transmissibility values as a function of frequency, values calculated as the ratio between the amplitudes measured in the two directions, for the two analyzed materials [21, 22].

At resonance, T_{max}=4.48 and the frequency is f_p=693.24 Hz.

The pulsation at resonance, p, calculated with the relation $p=2\pi fp$, results:

$$p = 2\pi * 693.24 = 4355.755\ rad/s$$

Knowing the maximum value of the transmissibility, the ordinate of the half-power points can be easily determined:

$$\frac{T_{max}}{\sqrt{2}} = \frac{4.48}{\sqrt{2}} = 3.1678$$

Knowing the ordinate of the half-power points and using the diagram in Figure 5, the frequencies corresponding to these points can be determined, as follows:

$$f_{p_1} = 594.27\ Hz\ respectively\ f_{p_2} = 789.57\ Hz$$

The pulsations corresponding to the half-power points are determined using the relation $\omega=2\pi f_p$ and results:

$$\omega_1 = 2\pi * f_{p_1} = 2\pi * 594.27 = 3733.91\ rad/s$$

respectively,

$$\omega_2 = 2\pi * f_{p_2} = 2\pi * 789.57 = 4961.01\ rad/s$$

The damping factor, g, for material C40 is calculated using the relation:

$$g = \frac{\omega_2^2 - \omega_1^2}{2p^2} = \frac{4961.01^2 - 3733.91^2}{2 \cdot 4355.755^2} = 0.281$$

The dynamic elastic constant of the analyzed material, k, calculated with relation (8), has the value:

$$k = mp^2 = 0.6 \cdot 4355.755^2 = 1.138 \cdot 10^7\ N/m$$

At resonance T_{max}=3.9265 and frequency f_p=235.865 Hz. The pulsation at resonance, p, is:

$$p = 2\pi * 235.865 = 1481.98\ rad/s$$

Knowing the maximum value of the transmissibility, the ordinate of the half-power points results:

$$\frac{T_{max}}{\sqrt{2}} = \frac{3.9265}{\sqrt{2}} = 2.776$$

Having determined the ordinate of the half-power points and using the diagram in Figure 5, the frequencies corresponding to the half-power points are obtained:

$$f_{p_1} = 216.48\ Hz\ respectively\ f_{p_2} = 256.13\ Hz$$

Using the relation $\omega=2\pi f_p$ results in the pulsations corresponding to the half-power points, as follows:

$$\omega_1 = 2\pi * f_{p_1} = 2\pi * 216.48 = 1360.18\ rad/s$$

respectively,

$$\omega_2 = 2\pi * f_{p_2} = 2\pi * 256.13 = 1609.31\ rad/s$$

The damping factor g for material C80 is:

$$g = \frac{\omega_2^2 - \omega_1^2}{2p^2} = \frac{1609.31^2 - 1360.18^2}{2 \cdot 1481.98^2} = 0.168$$

The dynamic elastic constant of the analyzed material C80, k, calculated with relation (8) has the value:

$$k = mp^2 = 0.6 \cdot 1481.98^2 = 0.13177 \cdot 10^7\ N/m$$

Using experimental data, Figure 8a and Figure 8c illustrate the variation of transmissibility as a function of frequency, with the mention that the experimentally determined values, both for frequency and for transmissibility, were recorded around the resonance [23, 24]. Using relation (19) and knowing the experimentally determined frequency values around the resonance, the phase shift diagram, φ, as a function of frequency, is illustrated in Figure 8b, for C40 and in Figure 8d, respectively for C80 material.

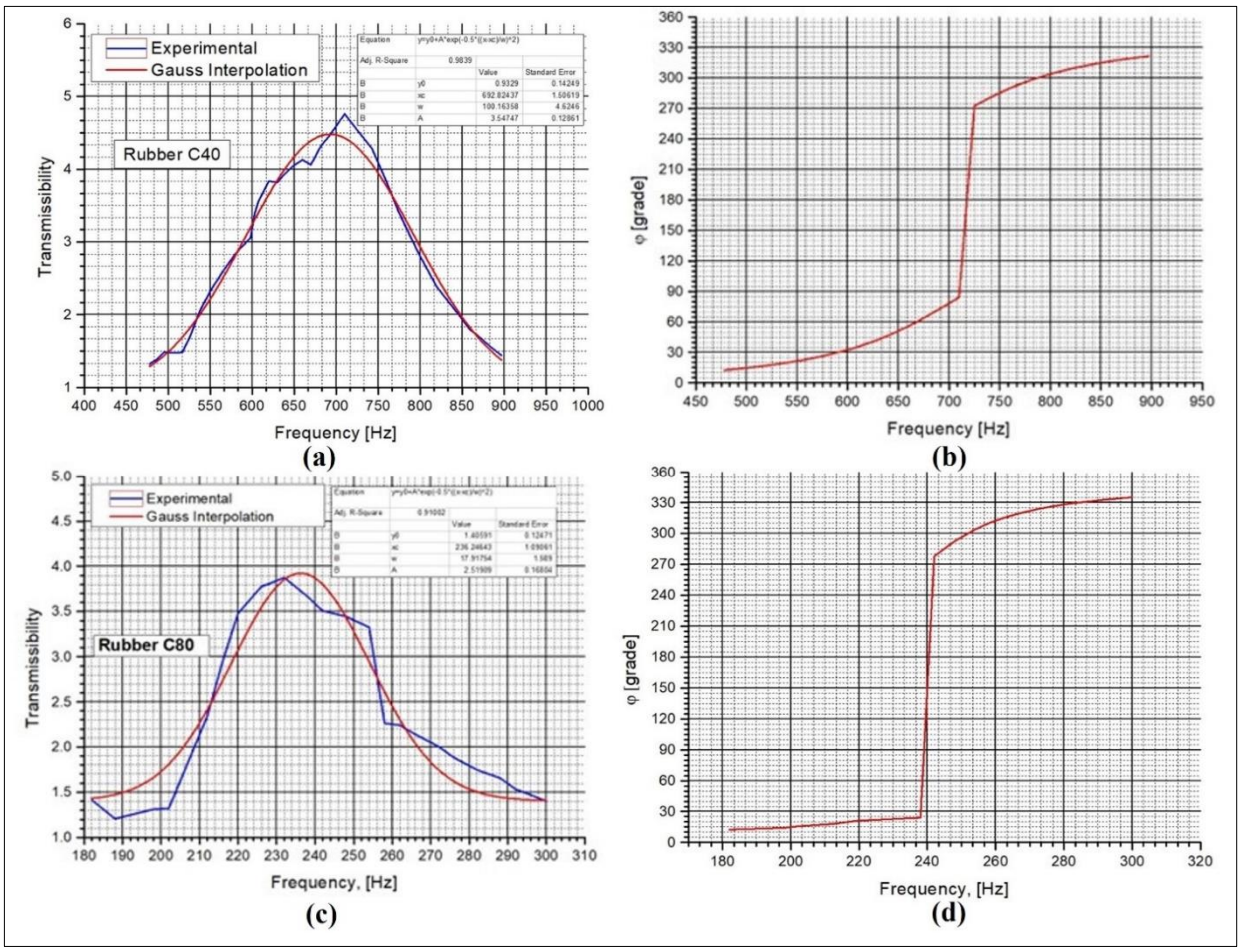

Figure 8. Experimental measurements of frequency-transmissibility: (a) Transmissibility - frequency diagram for C40; (b) Phase shift - frequency diagram for C40; (c) Transmissibility - frequency diagram for C80; (d) Phase shift - frequency diagram for C80

3.2. Determination of damping coefficient, *c*, for the analyzed materials

The damping coefficient is determined using the relation:

$$c = \frac{k}{\omega} \cdot g \tag{29}$$

The critical damping coefficient, c_{cr}, for the two studied materials, is determined with the relation:

$$c_{cr} = 2\sqrt{k \cdot m} = 2 \cdot p \cdot m \tag{30}$$

Knowing the mass of the elastic element m=0.6 kg and the resonance pulsations for each investigated material, the values of the critical damping coefficient c_{cr}, [Ns/m] are as follows: 5226.9 for C40 and 1778.4 for C80.

Using the experimental records made for the two types of materials and relation (29), the values of the damping coefficient as a function of frequency are determined.

Noting the ratio c/c_{cr} with ξ - relative damping, the variation of the damping coefficient as a function of frequency can be represented (Figure 9), for the two materials [25-27].

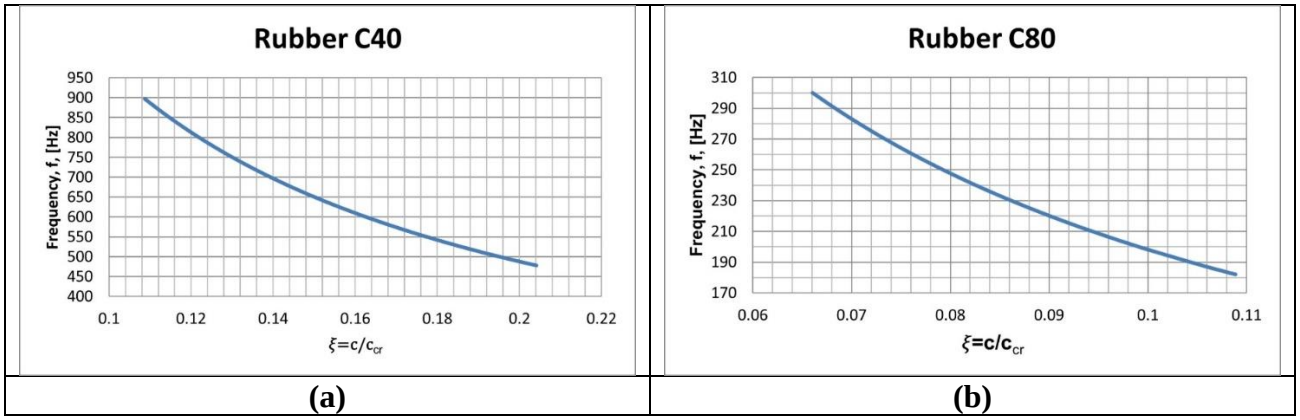

Figure 9. Variation of relative damping ξ as a function of frequency:
(a) C40 material; (b) C80 material

From the two graphs (Figure 9), it is concluded that the ratio c/c_{cr} lies between values 0 and 1, and the movement is in the form of an exponentially decreasing sinusoid [28-30].

4. Conclusions

In Figure 10, the results obtained through experimental determinations for pulsation at resonance, transmissibility at resonance, dynamic elastic constant and damping factor in the case of the two analyzed materials, are presented comparatively.

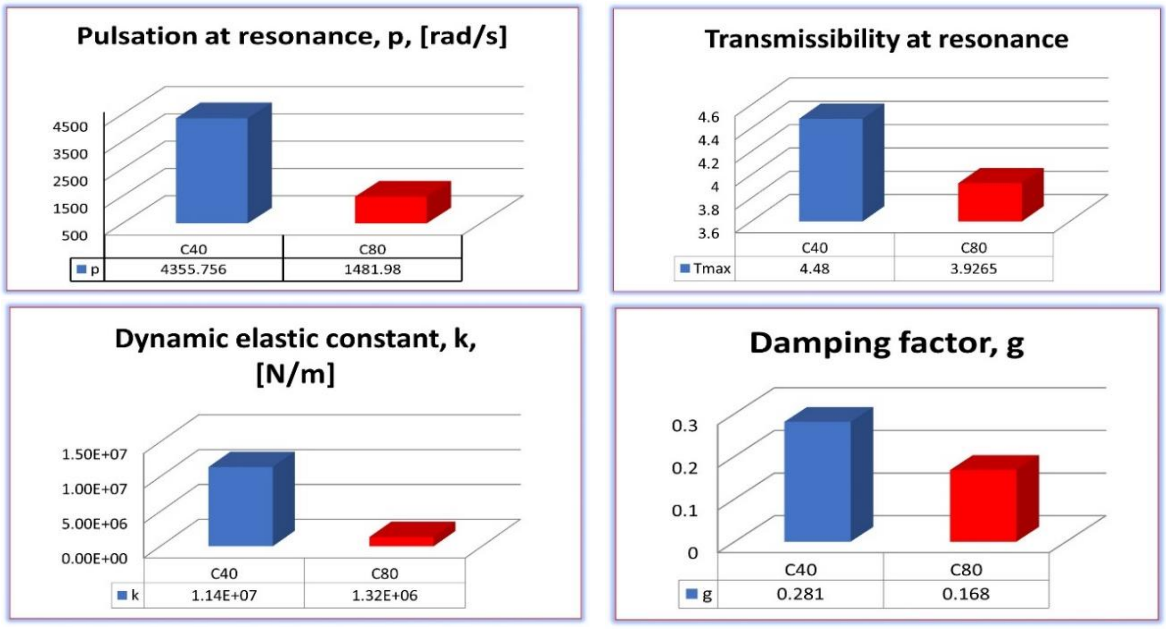

Figure 10. Dynamic characteristics obtained experimentally for C40 and C80 materials

Comparing the results obtained for pulsation at resonance of the samples made from the investigated materials, it is found that it decreases with the increase in the percentage of natural rubber in the composition.

Starting from the definition of transmissibility $T= F_{out}/ F_{in}$, it results that systems with high values of transmissibility are not effective in the case of foundations, because it is not desirable to transmit large forces in the foundation. In the case of couplings, a material with high transmissivity is useful because,

in their case, the damping capacity is of interest. In both cases, the stationary working regime must be considered, respectively the position of the working frequency with respect to $p\sqrt{2}$ (a value that delimits the supra-unitary regime from the sub-unitary regime of transmissibility).

The dynamic elastic constant k_d, calculated for the two investigated materials, is useful to perform a dynamic analysis for a system that has an elastic element of the nature of the studied materials, namely, a hyperelastic material.

From Figure 10, it is observed that the more elastic is the material, the lower is the dynamic constant, compared to the first material (C40) which has a lower percentage of natural rubber in its composition.

The large difference between the values of the elastic constant for these materials is a characteristic of hyperelastic materials in relation to elastic materials (for example steels), where the variation of the chemical composition results in a much smaller variation of this constant.

By analyzing the graph, can be concluded that the damping factor, for a material with a high percentage of natural rubber (>50%), is lower than in the case of a material with a low percentage of natural rubber [31]. In other words, a rubber with a high percentage of natural rubber dissipates less energy per unit of time, so it has lower damping properties, compared to one that has a lower amount of natural rubber in its composition.

References

1.KHANIKI, H.B., GHAYESH, M.H. et al., A review on the nonlinear dynamics of hyperelastic structures. Nonlinear Dynamics, **110**, 2022, 963-994.
2.OGDEN, R.W., Non-Linear Elastic Deformations, Dover Publications Mineola, New York, USA, 1997.
3.BOYCE, M.C., ARRUDA, E.M., Constitutive models of rubber elasticity: a review. Rubber Chemistry and Technology, **73**(3), 2000, 504-523.
4.TRELOAR, L.R.G., Stress-strain data for vulcanised rubber under various types of deformation. Trans. Faraday Soc., **40** (1944), 59-70.
5.MARCKMANN, G., VERRON, E., Comparison of Hyperelastic Models for Rubber-Like Materials. Rubber Chemistry and Technology, **79**, 2006, 835-858.
6.BERGSTRÖM, J., Elasticity/Hyperelasticity, Mechanics of Solid Polymers, Theory and Computational Modeling, William Andrew, 2015, 209-307.
7.MOONEY, M., A Theory of Large Elastic Deformation. J. Appl. Phys., **11**, 1940, 582-592.
8.YEOH, O.H., Some Forms of the Strain Energy Function for Rubber. Rubber Chem. Technol., **66**, 1993, 754-771.
9.KIM, B., LEE, S.B. et al., A comparison among Neo-Hookean model, Mooney-Rivlin model, and Ogden model for chloroprene rubber. Int. J. Precis. Eng. Manuf., **13**, 2012, 759-764.
10.UCAR, H., BASDOGAN, I., Dynamic characterization and modeling of rubber shock absorbers: A comprehensive case study. Journal of Low Frequency Noise, Vibration and Active Controls, **37**(3), 2018, 509-518.
11.MELLY, S.K., LIU, L., et al., A review on material models for isotropic hyperelasticity. IJMSD, **1**, 2021, 71-88.
12.SOMARATHNA, H.M.C.C., RAMAN, S.N. et al., Hyper-viscoelastic constitutive models for predicting the material behavior of polyurethane under varying strain rates and uniaxial tensile loading, Construction and Building Materials, **236**, 2020, 1-16.
13.WANG, F., LIAO, J., et al., Study on the Damping Dynamics Characteristics of a Viscoelastic Damping Material. Processes, **10**(4), 2022, 635, 1-15.
14.ROȘCA, I., Mechanical Vibrations, University of Transylvania, Brașov, Romania, 2009.
15.RADEȘ, M., Dynamic methods for the identification of mechanical systems, Academy of Romania, Bucharest 1979.

16.BRATU, P., JIGA, G., VLĂSCEANU, D., Methods for analyzing the dynamic performance of composite structural systems for the protective parapets equipping roadways. Proceedings of the Academy Days ASTR, Bucharest, Romania, 29th of November 2007.
17.PĂRĂUȘANU, I., Analysis of the dynamics of structures, Printech, Bucharest, Romania 2009.
18.AMIN, A.F.M.S., ALAM, M.S. et al., An improved hyperelasticity relation in modeling visco-elasticity response of natural and high damping rubbers in compression: experiments, parameter identification and numerical verification. Mech. Mater, **34**, 2002, 75-95.
19.AMIN, A.F.M.S, LION, A., et al., Nonlinear dependence of viscosity in modeling the rate-dependent response of natural and high damping rubbers in compression and shear: Experimental identification and numerical verification. Int. J. Plasticity, **22**, 2006, 1610-1657.
20.ZHAO, Z., YUAN, X. et al., Dynamical modeling and analysis of hyperelastic spherical shells under dynamic loads and structural damping. Applied Mathematical Modelling, **95**, 2021, 468-483.
21.ATANASIU, C., SOROHAN, S., Stress distribution in a coupling. JESI, **1**, 2009, 141-146.
22.ATANASIU, C., VLĂSCEANU, D. et al., The experimental investigations of residual stresses in tube with thick walls, Proceedings of DAAAM, **20**(1), 2009, 1163-1164.
23.BECHIR, H., CHEVALIER, L. et al., Hyperelastic constitutive model for rubber-like materials based on the first Seth strain measures invariant. EJM A/Solids, **25**, 2006, 110-124.
24.BERGSTROM, J.S., BOYCE, M.C., Constitutive modeling of the large strain time-dependent behavior of elastomers. JMPS, **46**, 1998, 931-954.
25. TABACU, ȘT., HADĂR, A., MARINESCU, D., IVĂNESCU, M., BALĂȘOIU, V., Numerical Procedures for the Improvement of the Structural Response of Thermoplastic Manufactured Parts, *Mater. Plast.*, **46**(2), 2009, 192-197.
26. VOICU, A.D., HADĂR, A., VLĂSCEANU, D., TUDOSE, D.I., Vibrational Study of a Helicopter Tail Rotor Blade with Different Polymer Inner Core Materials, *Mater. Plast.*, **57**(2), 2020, 169-178
27.PĂRĂUȘANU, I., Analysis of the dynamics of structures, Printech Bucharest, Romania, 2009.
28.RAPP, T., JACOBS, G. et al, Determining Dynamic Properties of Elastomer-Dampers by Means of Impact Testing, Exp Mech, **62**, 2022, 823-836.
29.GHARIB, M., KARKOUB, M., Design and experimental analysis of new industrial vibration dampers. J Mech Sci Technol, **32**, 2018, 3523-3535.
30.MASRI, S.F., Analytical and experimental studies of impact dampers, Ph.D. Thesis, California Institute of Technology, Pasadena, CA, USA, 1965.
31.VLĂSCEANU, D., Contributions regarding the mechanical behavior of axially symmetric structures made of hyperelastic materials Ph.D. Thesis, University Politehnica of Bucharest, Bucharest, Romania, 2011

Manuscript received: 19.02.2024